

Loop effect with vector mediator in the coherent neutrino-nucleus scattering

Wei Chao,^{1,*} Tong Li,^{2,†} Jiajun Liao,^{3,‡} and Min Su¹

¹*Center for Advanced Quantum Studies, Department of Physics,
Beijing Normal University, Beijing 100875, China*

²*School of Physics, Nankai University, Tianjin 300071, China*

³*School of Physics, Sun Yat-Sen University, Guangzhou 510275, China*

Abstract

The active neutrinos can convert into a new exotic fermion χ through coherent neutrino-nucleus scattering $\nu N \rightarrow \chi N$ and thus the $\nu - \chi$ interaction leads to novel recoil spectrum in the neutrino scattering experiments. We study the general neutrino interactions by evaluating both the tree-level and loop-level contributions to the coherent elastic neutrino-nucleus scattering (CE ν NS). The loop diagrams produce active neutrino elastic scattering process $\nu N \rightarrow \nu N$ with the fermion χ inside the loops. The neutrino interaction is illustrated by the framework of a simplified neutrino model in which a new Dirac fermion χ interacts with active neutrinos and a leptophobic vector mediator Z' . For the $Z'q\bar{q}$ coupling being vector type and axial-vector type, the CE ν NS processes are dominated by the tree-level and loop-level contribution, respectively. We investigate the constraints on the couplings between Z' and the new particle χ or the Standard Model quarks by fitting to the COHERENT data. The parameter space with m_χ larger than the maximal energy of incoming neutrinos can also be constrained by including the loop-level contribution. More importantly, the inclusion of loop diagrams can place constraint on axial-vector interaction whose the tree-level process is absent in the coherent neutrino-nucleus scattering.

* chaowei@bnu.edu.cn

† litong@nankai.edu.cn

‡ liaojiajun@mail.sysu.edu.cn

I. INTRODUCTION

The coherent elastic neutrino-nucleus scattering (CE ν NS) process was first observed by the COHERENT experiment [1] in the Spallation Neutron Source (SNS) at the Oak Ridge National Laboratory. The neutrinos measured at COHERENT are produced by the decays of stopped pion and muon with energies $E_\nu = (m_\pi^2 - m_\mu^2)/2m_\pi \simeq 30$ MeV and $E_\nu < m_\mu/2 \simeq 53$ MeV, respectively. For the neutrino-nucleus scattering, CE ν NS occurs when the momentum transfer in the process is smaller than the inverse of the target nucleus radius. The scattering amplitudes of the nucleons inside the nucleus can thus be summed all together coherently, which leads to a large enhancement of the cross section. The CE ν NS spectrum measured at COHERENT is consistent with the prediction of the Standard Model (SM), in which the CE ν NS process is generated through the weak neutral current [2]. Besides the active neutrinos through Z boson exchange in the SM, the CE ν NS process can also produce an exotic fermion such as the right-handed (RH) neutrinos without violating the coherence condition. Thus, the COHERENT observation can provide us an opportunity to explore the new physics (NP) associated with general neutrino interactions in the presence of exotic fermion.

Recently, different groups studied the conversion from active neutrinos to an exotic fermion χ in the coherent neutrino-nucleus scattering [3–6]

$$\nu N \rightarrow \chi N. \quad (1)$$

For this inelastic scattering process with $E_\nu < m_\mu/2$, the kinematic constraint on the mass of the exotic fermion χ becomes $m_\chi < \sqrt{M(m_\mu + M)} - M \simeq 53$ MeV with M being the nuclear mass [3, 4]. The COHERENT data can thus set bounds on this process only in the region of $m_\chi \lesssim 53$ MeV. On the other hand, the validation of the coherence in CE ν NS process depends on the specific interactions between neutrino and SM quark sector. Freedman et al. pointed out that the interactions such as axial quark current induce nuclear spin-dependent (SD) scattering and a cancellation between spin-up and spin-down nucleons [7]. They thus violate the coherence and the relevant CE ν NS processes are suppressed for all nuclei except for light ones. The observation for heavy CsI nuclei at COHERENT then can not place any constraint on the axial quark current and so on.

However, in the studies of the direct detection of WIMP dark matter (DM), it was emphasized that the interactions inducing SD scattering at tree-level can in turn generate spin-independent (SI) scattering through loop diagrams [8–24]. Moreover, the generated SI nuclear scattering cross section is independent of the momentum transfer $q \sim \mathcal{O}(\text{MeV})$ in the scattering and is not suppressed at leading order. The enhancement by the squared nuclear mass number in the coherent SI scattering compensates the suppression from the perturbative loop calculation. As a result, for the pseudoscalar or axial quark interaction, the full calculation involving the loop corrections would lead to sizable recoil events in DM direct detection experiments. We can apply the spirit of this loop effect to consider the loop corrections of the above inelastic neutrino scattering process [25]. Besides the tree-level $\nu N \rightarrow \chi N$ process, the loop diagrams produce active neutrino elastic scat-

tering process $\nu N \rightarrow \nu N$ with the above exotic fermion χ inside the loops. The involvement of loop diagrams would extend the constrained mass of fermion χ to $m_\chi > 53$ MeV because there is no kinematic bound on the internal fermion χ in $\nu N \rightarrow \nu N$ process. More importantly, the loop diagrams induce non-momentum-suppressed CE ν NS process and thus make the coupling of pseudoscalar or axial quark current become constrained by the COHERENT data. In this work we consider a simplified model of a fermionic particle χ interacting with SM neutrinos through a neutral vector boson Z' . The Z' boson interacts with SM quarks in a general form and we discuss the pure vector or axial-vector current between Z' and the SM quarks. The axial-vector interaction at tree-level in particular forbids the coherent neutrino-nucleus scattering. We investigate the SI elastic scattering generated by the loop corrections and the constraint on the model parameters by the COHERENT data.

This paper is organized as follows. In Sec. II we describe the simplified neutrino model with a vector mediator Z' . The Lagrangian is given in a general form with pure vector or axial-vector current for the interactions between Z' and the SM quarks. In Sec. III we present the analytical expressions of the CE ν NS cross section. Both the tree-level and loop-level contributions are given for the cases of vector and axial-vector currents. The numerical constraints on the couplings by the COHERENT data are also shown in Sec. IV. Our conclusions are drawn in Sec. V. The details of loop calculations are collected in the Appendix.

II. SIMPLIFIED NEUTRINO MODEL WITH A VECTOR MEDIATOR

A. The simplified model

We study a simplified model of a Dirac fermionic particle χ interacting with SM neutrino and a neutral vector boson Z' after the electroweak symmetry breaking. The Lagrangian is given by

$$\mathcal{L} \supset Z'_\mu \bar{\chi} \gamma^\mu (g_{\chi L} P_L + g_{\chi R} P_R) \nu + Z'_\mu \sum_q \bar{q} \gamma^\mu (g_{qL} P_L + g_{qR} P_R) q + h.c., \quad (2)$$

where the Z' is assumed to be leptophobic and the quark couplings g_{qL}, g_{qR} are not flavor universal. The massive gauge field Z' is associated with a pseudo-Nambu Goldstone boson (pNGB) φ . The Yukawa interaction of fermions with φ is given by [26]

$$\mathcal{L} \supset \varphi \frac{-i}{m_{Z'}} m_\chi \bar{\chi} (g_{\chi L} P_L + g_{\chi R} P_R) \nu + \varphi \frac{i}{m_{Z'}} m_q \bar{q} ((g_{qR} - g_{qL}) P_L + (g_{qL} - g_{qR}) P_R) q + h.c. \quad (3)$$

in the limit of massless neutrino. We use the Feynman-'tHooft gauge to calculate the diagrams below.

We further define two scenarios of the quark couplings

- Case A: $g_{qL} = g_{qR} = g_q$
- Case B: $g_{qL} = -g_{qR} = g_q$

and assume the couplings of all quark species are not universal. The choice of case A is exactly the case with pure vector interaction between Z' and the SM quark sector. In this case the Yukawa interaction involving the pNGB φ is absent. It leads to the SI neutrino-nucleus scattering $\nu N \rightarrow \chi N$ at tree-level and the COHERENT data can place constraint on the interaction for $m_\chi \lesssim 53$ MeV. By contrast, the case B induces the axial-vector interaction at tree-level, i.e. $Z'_\mu \bar{q} \gamma^\mu \gamma_5 q$, and the corresponding SD neutrino-nucleus scattering is absent in CE ν NS process. The relevant tree-level inelastic scattering can not be constrained by COHERENT data. We next consider the loop corrections for the two scenarios and the $\nu N \rightarrow \nu N$ process constrained by COHERENT data.

B. Constraints

The simplified neutrino model can be constrained by the invisible rare decays such as $K^+ \rightarrow \pi^+ + \text{invisible}$ via flavor changing neutral currents [27]. This rare decay process is recently measured by the NA62 experiment at CERN [28]. The actual calculation of the decay rate would suffer from a problem of UV divergence due to the fact that the simplified model here is not gauge-invariant [12, 27]. The reliable estimate of the flavor observable relies on the UV completion realization. As the $K \rightarrow \pi$ transitions are induced by flavor changing neutral currents, they set stringent constraints on g_q coupling for up-type quarks [5, 25]. We thus assume non-universal g_q couplings for up-type and down-type quarks and neglect the up-type quark coupling in the following calculations. The UV problem does not affect our assumption of the couplings below and the corresponding conclusions.

Another constraint on the model is the effective number of relativistic neutrino species N_{eff} in the early Universe, where N_{eff} is defined by

$$N_{eff} = \frac{8}{7} \left(\frac{11}{4} \right)^3 \left(\frac{\rho_{rad} - \rho_\gamma}{\rho_\gamma} \right) \quad (4)$$

with ρ_{rad} and ρ_γ being the total radiation and photon energy densities, respectively. Considering the neutrino decoupling in the minimal SM, one has $N_{eff}^{SM} = 3.043 \sim 3.045$ [29–31]. Deviation from the SM prediction can be measured by CMB observations and the CMB Stage IV experiments are expected to reach a precision of $\Delta N = N_{eff} - N_{eff}^{SM} \sim 0.03$ [32, 33] in the future. In our model, the thermal history of active neutrinos might be modified by the portal-like interaction in Eq. (3), depending on parameter settings of the new coupling and masses of new species. For $m_\chi, m_{Z'} \gg \mathcal{O}(1)$ MeV, new species already decay away at the time of neutrino decoupling, and any deviation from the N_{eff}^{SM} will be washed-out by weak interactions since neutrinos are still in thermal equilibrium with photon and electron at time of decays. Alternatively, if $m_\chi, m_{Z'} \leq \mathcal{O}(1)$ MeV, N_{eff}^{SM} can be modified by the new interaction. However, this parameter space is not favored by the CE ν NS, as can be seen from the Fig. 4 in Sec. IV, and χ is similar to be a short-lived FIMP [34] in this case. Since we mainly focus on CE ν NS in this paper, a systematic study of the impaction of this model to N_{eff} will be presented in another work.

III. COHERENT ELASTIC NEUTRINO-NUCLEUS SCATTERING

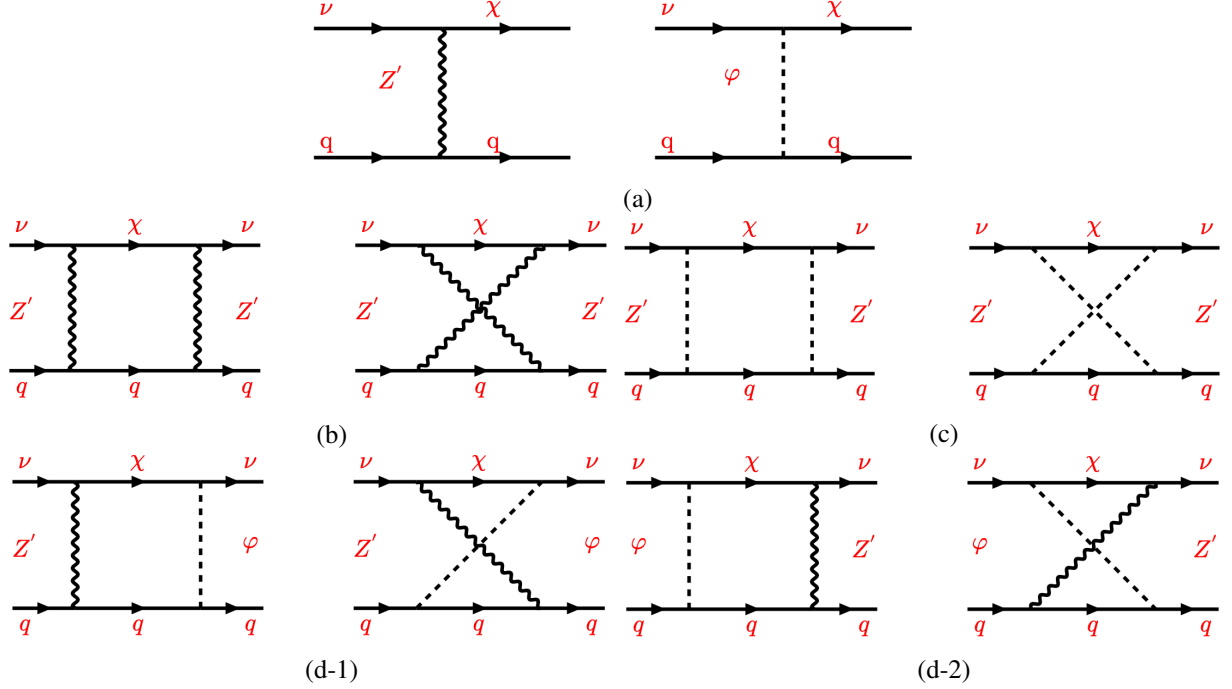


FIG. 1. Diagrams for the scattering processes of neutrino, (a): tree-level diagrams, (b): box diagrams with Z' as mediator, (c): box diagrams with the pNGB φ as mediator, (d): box diagrams with Z' - φ as mediator.

In this section we evaluate the coherent neutrino-nucleus scattering induced by the two coupling choices at both tree-level and loop-level. We first derive the scattering matrix elements at quark level. For $\nu(p_1)q(k_1) \rightarrow \chi(p_2)q(k_2)$ as shown in Fig. 1 (a), we obtain the general tree-level matrix element

$$i\mathcal{M}_{\text{tree}} = \sum_{q=\text{all}} \frac{i}{t - m_{Z'}^2} \bar{\chi}(p_2) \gamma_\mu g_{\chi L} P_L \nu(p_1) \bar{q}(k_2) \gamma^\mu (g_{qL} P_L + g_{qR} P_R) q(k_1) \\ + \sum_{q=\text{all}} \frac{-im_\chi m_q}{m_{Z'}^2} \bar{\chi}(p_2) g_{\chi L} P_L \nu(p_1) \bar{q}(k_2) \left[(g_{qR} - g_{qL}) P_L + (g_{qL} - g_{qR}) P_R \right] q(k_1), \quad (5)$$

with the Mandelstam variable $t = (p_1 - p_2)^2$. For case A the first term induces vector current $\bar{q}\gamma^\mu q$ and the second term vanishes. The two terms result in either axial-vector or pseudo-scalar current in case B.

The elastic scattering process $\nu(p_1)q(k_1) \rightarrow \nu(p_2)q(k_2)$ occurs through multiple loop-level contributions to the leading SI effective operators. The SI effective operators decompose into the scalar operator $\bar{\nu}\nu\bar{q}q$, the twist-2 neutrino-quark operators and the neutrino-gluon scalar operator $\bar{\nu}\nu G_{\mu\nu}^a G^{a\mu\nu}$. The one-loop box diagrams in Fig. 1 contribute to the scalar operator with each of the light quarks u, d, s as well as the twist-2 operators for $q = u, d, s, c, b$. The cases A and B both

have one-loop box diagrams with the vector mediator Z' as shown in Fig. 1 (b)

$$\begin{aligned}
i\mathcal{M}_{\text{box}-Z'Z'} = & - \sum_{q=u,d,s} \frac{i}{(4\pi)^2} g_{\chi L} g_{\chi R} g_q^2 m_\chi m_q \left[\kappa D_0^b + \frac{8}{m_{Z'}^2} (D_{00}^a - D_{00}^b) \right] \bar{\nu}(p_2) P_L \nu(p_1) \bar{q}(k_2) q(k_1) \\
& + \sum_{q=u,d,s,c,b} \frac{i}{(4\pi)^2} g_{\chi L}^2 g_q^2 \left[\frac{16}{m_{Z'}^2} (4D_{001}^a - 4D_{001}^b + D_{00}^a - D_{00}^b) + 8(D_1^b + D_0^b) \right] \bar{\nu}(p_2) i\partial^\mu \gamma^\nu P_L \nu(p_1) \mathcal{O}_{\mu\nu}^q \\
& - \sum_{q=u,d,s,c,b} \frac{i}{(4\pi)^2} g_{\chi L} g_{\chi R} g_q^2 \frac{8}{m_{Z'}^2} m_\chi (D_{11}^a - D_{11}^b) \bar{\nu}(p_2) i\partial^\mu i\partial^\nu P_L \nu(p_1) \mathcal{O}_{\mu\nu}^q, \tag{6}
\end{aligned}$$

where $\kappa = -4$ (12) for case A (B) and $\mathcal{O}_{\mu\nu}^q$ is the twist-2 operator for quark

$$\mathcal{O}_{\mu\nu}^q = \frac{i}{2} \bar{q} \left(\partial_\mu \gamma_\nu + \partial_\nu \gamma_\mu - \frac{1}{2} g_{\mu\nu} \not{\partial} \right) q. \tag{7}$$

The Passarino-Veltman functions used here and below are collected in the Appendix. The case B has additional contributions involving the pNGB φ as shown in Figs. 1 (c) and (d). The matrix element of the one-loop box diagrams with the would-be Goldstone mediator φ is

$$\begin{aligned}
i\mathcal{M}_{\text{box}-\varphi\varphi}(\text{B}) = & - \sum_{q=u,d,s} \frac{i}{(4\pi)^2} g_q^2 g_{\chi L} g_{\chi R} \frac{32m_\chi^3 m_q^3}{m_{Z'}^6} (D_{00}^a - D_{00}^b) \bar{\nu}(p_2) P_L \nu(p_1) \bar{q}(k_2) q(k_1) \\
& - \sum_{q=u,d,s,c,b} \frac{i}{(4\pi)^2} g_q^2 g_{\chi L}^2 \frac{64m_\chi^2 m_q^2}{m_{Z'}^6} (D_{001}^a - D_{001}^b) \bar{\nu}(p_2) i\partial^\mu \gamma^\nu P_L \nu(p_1) \mathcal{O}_{\mu\nu}^q \\
& - \sum_{q=u,d,s,c,b} \frac{i}{(4\pi)^2} g_q^2 g_{\chi L} g_{\chi R} \frac{32m_\chi^3 m_q^2}{m_{Z'}^6} (D_{11}^a - D_{11}^b) \bar{\nu}(p_2) i\partial^\mu i\partial^\nu P_L \nu(p_1) \mathcal{O}_{\mu\nu}^q \tag{8}
\end{aligned}$$

The one-loop box diagrams of the Z' - φ mixing mediator induce the following matrix element

$$i\mathcal{M}_{\text{box}-Z'\varphi}(\text{B}) = \sum_{q=u,d,s} \frac{i}{(4\pi)^2} g_q^2 g_{\chi L} g_{\chi R} \frac{32m_\chi m_q}{m_{Z'}^2} D_{00}^b \bar{\nu}(p_2) P_L \nu(p_1) \bar{q}(k_2) q(k_1). \tag{9}$$

The contributions of heavy quarks should be integrated out at the two-loop level and cause the effective interaction between neutrino and gluon fields with the same order of magnitude. For heavy quarks running in two-loop diagrams in Fig. 2, we calculate the amplitude using the Fock-Schwinger gauge [35–38] for the gluon background field in zero momentum limit [9, 14, 39, 40]. The complete two-loop matrix elements with two Z' running in the loop in the Fig. 2 read as follows

$$i\mathcal{M}_{2\text{loop}-Z'Z'} = \kappa' \sum_{q=c,b} \frac{i}{(4\pi)^2} \frac{\alpha_s}{12\pi} G_{\alpha\beta}^a G^{a\alpha\beta} g_q^2 g_{\chi L} g_{\chi R} m_\chi D_0^b \bar{\nu}(p_2) P_L \nu(p_1), \tag{10}$$

where $G_{\alpha\beta}^a$ is the gluon field strength tensor and $\kappa' = -3$ (13) for case A (B). The contribution from the top quark loop is suppressed by the top quark mass and we neglect its contribution in our

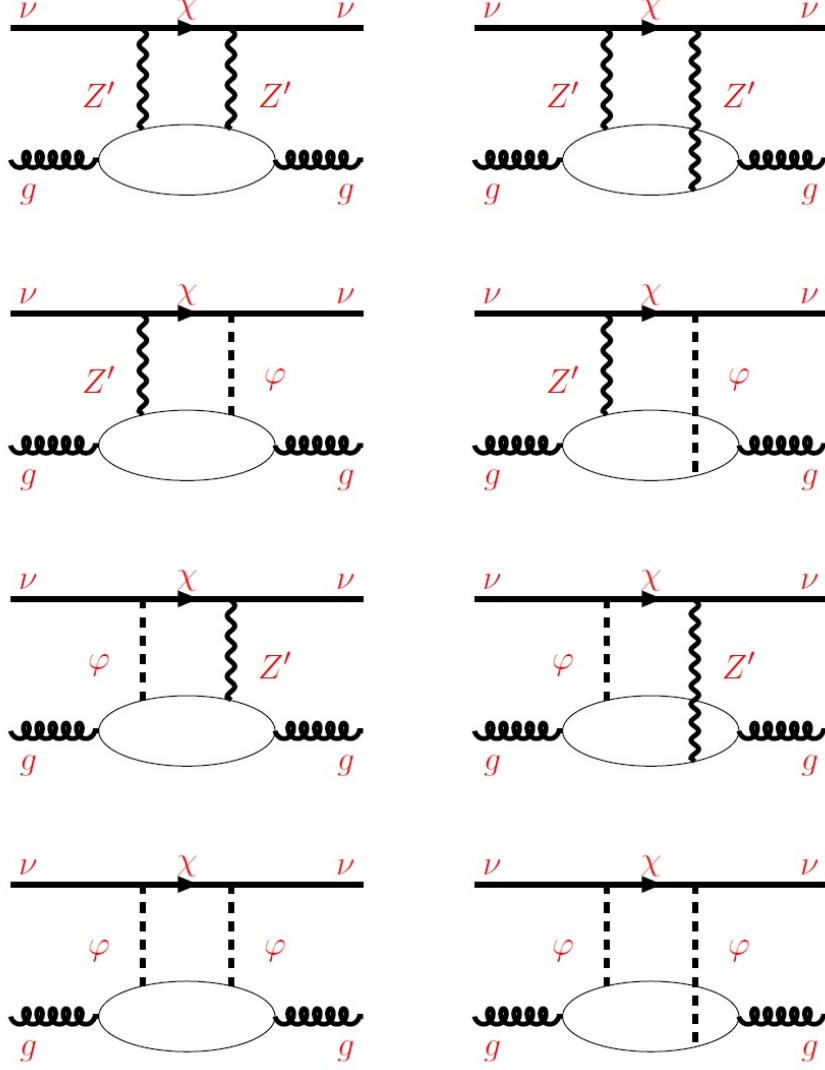


FIG. 2. Two-loop diagrams for effective gluon interactions with Z' and pNGB φ mediators.

numerical calculation. For case B, there is additional contribution from two pNGB mediators in the loop

$$i\mathcal{M}_{2\text{loop}-\varphi\varphi}(\text{B}) = - \sum_{q=c,b,t} \frac{i}{(4\pi)^2} \frac{\alpha_s}{12\pi} G_{\alpha\beta}^a G^{a\alpha\beta} \frac{2g_q^2 m_q^2 m_\chi^3}{m_{Z'}^4} g_{\chi L} g_{\chi R} \frac{\partial}{\partial m_{Z'}^2} F_G(m_{Z'}^2) \bar{\nu}(p_2) P_L \nu(p_1), \quad (11)$$

where the F_G function is also collected in Appendix. As we adopt downphilic coupling g_q , in the numerical calculation, we neglect the two-loop diagrams dominated by top quark contribution. For Z' - φ mixing mediators, the two-loop contribution vanishes.

Next, we can obtain the matrix elements at nucleon-level in terms of the nucleon form factors.

The nucleon form factors are defined as [41, 42]

$$\langle N|m_q \bar{q}q|N\rangle = m_N f_q^N \bar{N}N, \quad q = u, d, s, \quad (12)$$

$$\langle N|m_Q \bar{Q}Q|N\rangle = \langle N|\frac{-\alpha_s}{12\pi} G_{\mu\nu}^a G^{a\mu\nu}|N\rangle = \frac{2}{27} m_N f_G^N \bar{N}N, \quad Q = c, b, t, \quad (13)$$

$$\langle N|\mathcal{O}_{\mu\nu}^q|N\rangle = \frac{1}{m_N} \left(p_\mu^N p_\nu^N - \frac{1}{4} m_N^2 g_{\mu\nu} \right) \left(q^N(2) + \bar{q}^N(2) \right) \bar{N}N, \quad q = u, d, s, c, b, \quad (14)$$

$$\langle N|\bar{q}\gamma^\mu q|N\rangle = c_q^N \bar{N}\gamma^\mu N, \quad c_u^p = c_d^p = 2, c_d^n = c_u^n = 1, c_s^n = c_s^p = 0, \quad (15)$$

for the SI interactions. The nucleon-level tree diagram of $\nu N \rightarrow \chi N$ then becomes

$$\begin{aligned} i\mathcal{M}_{\text{tree}}^N &= \sum_{q=u,d,s} \frac{i}{t - m_{Z'}^2} \frac{g_{\chi L}(g_{qL} + g_{qR})}{2} c_q^N \bar{\chi}(p_2) \gamma_\mu P_L \nu(p_1) \bar{N}(k_2) \gamma^\mu N(k_1) + \boxed{\text{SD}} \\ &= \begin{cases} \sum_{q=u,d,s} c_q^N \frac{i}{t - m_{Z'}^2} g_{\chi L} g_q \bar{\chi}(p_2) \gamma_\mu P_L \nu(p_1) \bar{N}(k_2) \gamma^\mu N(k_1), & \text{case A} \\ 0, & \text{case B} \end{cases} + \boxed{\text{SD}}, \quad (16) \end{aligned}$$

where $\boxed{\text{SD}}$ stands for SD terms which will be omitted in the following calculation. The nucleon-level box diagrams for $\nu N \rightarrow \nu N$ are

$$\begin{aligned} i\mathcal{M}_{\text{box}-Z'Z'}^N &= -\frac{i}{(4\pi)^2} g_{\chi L} g_{\chi R} g_q^2 m_\chi \bar{\nu}(p_2) P_L \nu(p_1) \bar{N}(k_2) N(k_1) \\ &\quad \times \left[\kappa D_0^b + \frac{8}{m_{Z'}^2} (D_{00}^a - D_{00}^b) \right] \left(\sum_{q=u,d,s} m_N f_q^N \right) \\ &\quad + \frac{i}{(4\pi)^2} g_{\chi L}^2 g_q^2 \frac{(k_1 \cdot p_1)}{m_N} \bar{\nu}(p_2) \not{k}_1 P_L \nu(p_1) \bar{N}(k_2) N(k_1) \sum_{q=u,d,s,c,b} (q^N(2) + \bar{q}^N(2)) \\ &\quad \times \left[\frac{16}{m_{Z'}^2} (4D_{001}^a - 4D_{001}^b + D_{00}^a - D_{00}^b) + 8(D_1^b + D_0^b) \right] \\ &\quad - \frac{i}{(4\pi)^2} g_{\chi L} g_{\chi R} g_q^2 \frac{8}{m_{Z'}^2} m_\chi \frac{(k_1 \cdot p_1)^2}{m_N} \bar{\nu}(p_2) P_L \nu(p_1) \bar{N}(k_2) N(k_1) \\ &\quad \times (D_{11}^a - D_{11}^b) \sum_{q=u,d,s,c,b} (q^N(2) + \bar{q}^N(2)), \quad (17) \end{aligned}$$

$$i\mathcal{M}_{\text{box}-Z'\varphi}^N(\text{B}) = \frac{i}{(4\pi)^2} g_q^2 g_{\chi L} g_{\chi R} \frac{32m_\chi}{m_{Z'}^2} D_{00}^b \left(\sum_{q=u,d,s} m_N f_q^N \right) \bar{\nu}(p_2) P_L \nu(p_1) \bar{N}(k_2) N(k_1), \quad (18)$$

$$\begin{aligned} i\mathcal{M}_{\text{box}-\varphi\varphi}^N(\text{B}) &= -\frac{i}{(4\pi)^2} g_q^2 g_{\chi L} g_{\chi R} \frac{32m_\chi^3}{m_{Z'}^6} \bar{\nu}(p_2) P_L \nu(p_1) \bar{N}(k_2) N(k_1) \\ &\quad \times (D_{00}^a - D_{00}^b) \left(\sum_{q=u,d,s} m_N m_q^2 f_q^N \right) \\ &\quad - \frac{i}{(4\pi)^2} g_q^2 g_{\chi L}^2 \frac{64m_\chi^2}{m_{Z'}^6} \frac{(k_1 \cdot p_1)}{m_N} \bar{\nu}(p_2) \not{k}_1 P_L \nu(p_1) \bar{N}(k_2) N(k_1) \end{aligned}$$

$$\begin{aligned}
& \times (D_{001}^a - D_{001}^b) \sum_{q=u,d,s,c,b} m_q^2 (q^N(2) + \bar{q}^N(2)) \\
& - \frac{i}{(4\pi)^2} g_q^2 g_{\chi L} g_{\chi R} \frac{32m_\chi^3}{m_{Z'}^6} \frac{(k_1 \cdot p_1)^2}{m_N} \bar{\nu}(p_2) P_L \nu(p_1) \bar{N}(k_2) N(k_1) \\
& \times (D_{11}^a - D_{11}^b) \sum_{q=u,d,s,c,b} m_q^2 (q^N(2) + \bar{q}^N(2)) .
\end{aligned} \tag{19}$$

The non-vanishing two-loop matrix elements are given by

$$i\mathcal{M}_{2\text{loop}-Z'Z'}^N = -\kappa' \sum_{q=c,b} \frac{i}{(4\pi)^2} g_q^2 g_{\chi L} g_{\chi R} m_\chi \frac{2}{27} m_N f_G^N D_0^b \bar{\nu}(p_2) P_L \nu(p_1) \bar{N}(k_2) N(k_1) , \tag{20}$$

with $\kappa' = -3$ (13) for case A (B) and

$$\begin{aligned}
i\mathcal{M}_{2\text{loop}-\varphi\varphi}^N(\text{B}) &= \sum_{q=c,b,t} \frac{i}{(4\pi)^2} \frac{2g_q^2 m_q^2 m_\chi^3}{m_{Z'}^4} g_{\chi L} g_{\chi R} \frac{2}{27} m_N f_G^N F_G(p_1^2, m_\chi^2, m_{Z'}^2, m_q^2) \\
&\times \bar{\nu}(p_2) P_L \nu(p_1) \bar{N}(k_2) N(k_1) .
\end{aligned} \tag{21}$$

Since only the nuclear recoil is detected in a neutrino scattering experiment, the total differential cross section of CE ν NS can be written as

$$\frac{d\sigma}{dT} = \frac{d\sigma_{\text{SM}}}{dT} + \frac{d\sigma_{\text{tree}}}{dT} + \frac{d\sigma_{\text{loop}}}{dT} , \tag{22}$$

where T denotes the nuclear recoil energy. The differential cross section in the SM is given by

$$\frac{d\sigma_{\text{SM}}}{dT} = \frac{G_F^2 M}{2\pi} [Zg_p^V + Ng_n^V]^2 F^2(Q^2) \left(2 - \frac{MT}{E^2} - \frac{2T}{E} + \frac{T^2}{E^2} \right) , \tag{23}$$

where E denotes the incoming neutrino energy, Z (N) is the number of protons (neutrons) in the target nucleus, $g_n^V = -\frac{1}{2}$ and $g_p^V = \frac{1}{2} - 2\sin^2\theta_W$ are the SM weak couplings with θ_W being the weak mixing angle. Here $F(Q^2)$ represents the nuclear form factor with the moment transfer $Q^2 = 2MT$. Since different form factor parameterizations have a negligible effect on the COHERENT spectrum [43, 44], we take the Helm parameterization [45] for the nuclear form factor in our analysis.

From Eq. (16), the tree-level differential cross section of $\nu N \rightarrow \chi N$ for case A is

$$\begin{aligned}
\frac{d\sigma_{\text{tree}}}{dT} &= \frac{g_{\chi L}^2 M F^2(Q^2)}{4\pi(m_{Z'}^2 + 2MT)^2} \left[(2g_u + g_d)Z + (g_u + 2g_d)N \right]^2 \\
&\left[\left(2 - \frac{MT}{E^2} - \frac{2T}{E} + \frac{T^2}{E^2} \right) - \frac{m_\chi^2}{2E^2} \left(1 + 2\frac{E}{M} - \frac{T}{M} \right) \right] .
\end{aligned} \tag{24}$$

For case B, the tree-level differential cross section of $\nu N \rightarrow \chi N$ is zero. Note that in order to produce a massive fermion χ in the scattering $\nu N \rightarrow \chi N$, the energy of the incident neutrinos should be larger than a minimal energy [3, 4], i.e.,

$$E > m_\chi + \frac{m_\chi^2}{2M} . \tag{25}$$

From Eqs. (17), (18), (19), (20) and (21), we can write the loop-level differential cross section of $\nu N \rightarrow \nu N$ as

$$\frac{d\sigma_{\text{loop}}}{dT} = \frac{M^3}{8\pi} F^2(Q^2) (2M + T) \left[T \left(\frac{c_1}{ME} + c_3 ME \right)^2 + c_2^2 (2ME(E - T) - M^2 T) \right], \quad (26)$$

where

$$c_1 = -\frac{1}{(4\pi)^2} g_{\chi L} g_{\chi R} m_\chi \left[\kappa D_0^b + \frac{8}{m_{Z'}^2} (D_{00}^a - D_{00}^b) \right] \sum_{q=u,d,s} g_q^2 (Z m_p f_q^p + N m_n f_q^n) \\ - \kappa' \frac{1}{(4\pi)^2} g_{\chi L} g_{\chi R} m_\chi \frac{2}{27} D_0^b \sum_{q=c,b} g_q^2 (Z m_p f_G^p + N m_n f_G^n), \quad (27)$$

$$c_2 = \frac{1}{(4\pi)^2} g_{\chi L}^2 \left[\frac{16}{m_{Z'}^2} (4D_{001}^a - 4D_{001}^b + D_{00}^a - D_{00}^b) + 8(D_1^b + D_0^b) \right] \\ \times \sum_{q=u,d,s,c,b} g_q^2 \left[\frac{Z}{m_p} (q^p(2) + \bar{q}^p(2)) + \frac{N}{m_n} (q^n(2) + \bar{q}^n(2)) \right], \quad (28)$$

$$c_3 = -\frac{1}{(4\pi)^2} g_{\chi L} g_{\chi R} \frac{8m_\chi}{m_{Z'}^2} (D_{11}^a - D_{11}^b) \sum_{q=u,d,s,c,b} g_q^2 \left[\frac{Z}{m_p} (q^p(2) + \bar{q}^p(2)) + \frac{N}{m_n} (q^n(2) + \bar{q}^n(2)) \right], \quad (29)$$

for case A, and

$$c_1 = -\frac{1}{(4\pi)^2} g_{\chi L} g_{\chi R} m_\chi \left[\kappa D_0^b + \frac{8}{m_{Z'}^2} (D_{00}^a - D_{00}^b) \right] \sum_{q=u,d,s} g_q^2 (Z m_p f_q^p + N m_n f_q^n) \\ + \frac{1}{(4\pi)^2} g_{\chi L} g_{\chi R} \frac{32m_\chi}{m_{Z'}^2} D_{00}^b \sum_{q=u,d,s} g_q^2 (Z m_p f_q^p + N m_n f_q^n) \\ - \frac{1}{(4\pi)^2} g_{\chi L} g_{\chi R} \frac{32m_\chi^3}{m_{Z'}^6} (D_{00}^a - D_{00}^b) \sum_{q=u,d,s} g_q^2 m_q^2 (Z m_p f_q^p + N m_n f_q^n) \\ - \kappa' \frac{1}{(4\pi)^2} g_{\chi L} g_{\chi R} m_\chi \frac{2}{27} D_0^b \sum_{q=c,b} g_q^2 (Z m_p f_G^p + N m_n f_G^n) \\ + \frac{1}{(4\pi)^2} g_{\chi L} g_{\chi R} \frac{m_\chi^3}{m_{Z'}^4} \frac{4}{27} \sum_{q=c,b,t} g_q^2 m_q^2 F_G(p_1^2, m_\chi^2, m_{Z'}^2, m_q^2) (Z m_p f_G^p + N m_n f_G^n), \quad (30)$$

$$c_2 = \frac{1}{(4\pi)^2} g_{\chi L}^2 \left[\frac{16}{m_{Z'}^2} (4D_{001}^a - 4D_{001}^b + D_{00}^a - D_{00}^b) + 8(D_1^b + D_0^b) \right] \\ \times \sum_{q=u,d,s,c,b} g_q^2 \left[\frac{Z}{m_p} (q^p(2) + \bar{q}^p(2)) + \frac{N}{m_n} (q^n(2) + \bar{q}^n(2)) \right] \\ - \frac{1}{(4\pi)^2} g_{\chi L}^2 \frac{64m_\chi^2}{m_{Z'}^6} (D_{001}^a - D_{001}^b) \\ \times \sum_{q=u,d,s,c,b} g_q^2 m_q^2 \left[\frac{Z}{m_p} (q^p(2) + \bar{q}^p(2)) + \frac{N}{m_n} (q^n(2) + \bar{q}^n(2)) \right], \quad (31)$$

$$c_3 = -\frac{1}{(4\pi)^2} g_{\chi L} g_{\chi R} \frac{8m_\chi}{m_{Z'}^2} (D_{11}^a - D_{11}^b)$$

$$\begin{aligned}
& \times \sum_{q=u,d,s,c,b} \left[\frac{Z}{m_p} (q^p(2) + \bar{q}^p(2)) + \frac{N}{m_n} (q^n(2) + \bar{q}^n(2)) \right] \\
& - \frac{1}{(4\pi)^2} g_{\chi L} g_{\chi R} \frac{32m_\chi^3}{m_{Z'}^6} (D_{11}^a - D_{11}^b) \\
& \times \sum_{q=u,d,s,c,b} g_q^2 m_q^2 \left[\frac{Z}{m_p} (q^p(2) + \bar{q}^p(2)) + \frac{N}{m_n} (q^n(2) + \bar{q}^n(2)) \right], \tag{32}
\end{aligned}$$

for case B. One can see that the coefficients c_1 are from both quark and gluon scalar operators. The coefficients c_2, c_3 are only dependent on the twist-2 operator. For the nucleon form factors in SI interactions, we adopt the default values in micrOMEGAs [46, 47].

The neutrinos measured at COHERENT are generated from the stopped pion decays and the muon decays, and their fluxes are given by

$$\begin{aligned}
\phi_{\nu_\mu}(E_{\nu_\mu}) &= \mathcal{N}_0 \frac{2m_\pi}{m_\pi^2 - m_\mu^2} \delta \left(1 - \frac{2E_{\nu_\mu} m_\pi}{m_\pi^2 - m_\mu^2} \right), \\
\phi_{\nu_e}(E_{\nu_e}) &= \mathcal{N}_0 \frac{192}{m_\mu} \left(\frac{E_{\nu_e}}{m_\mu} \right)^2 \left(\frac{1}{2} - \frac{E_{\nu_e}}{m_\mu} \right), \\
\phi_{\bar{\nu}_\mu}(E_{\bar{\nu}_\mu}) &= \mathcal{N}_0 \frac{64}{m_\mu} \left(\frac{E_{\bar{\nu}_\mu}}{m_\mu} \right)^2 \left(\frac{3}{4} - \frac{E_{\bar{\nu}_\mu}}{m_\mu} \right), \tag{33}
\end{aligned}$$

where the normalization factor $\mathcal{N}_0 = \frac{rtN_{\text{POT}}}{4\pi L^2}$ with $r = 0.08$ being the number of neutrinos per flavor produced per proton collision, t the number of years of data collection, $N_{\text{POT}} = 2.1 \times 10^{23}$ the total number of protons on target per year, and L the distance between the source and the detector [1]. The ν_μ component is produced from the stopped pion decays, $\pi^+ \rightarrow \mu^+ + \nu_\mu$, with a monoenergetic flux at $(m_\pi^2 - m_\mu^2)/(2m_\pi) \simeq 30$ MeV. The $\bar{\nu}_\mu$ and ν_e components are produced from the subsequent muon decays, $\mu^+ \rightarrow e^+ + \bar{\nu}_\mu + \nu_e$, with a kinematic upper bound at $m_\mu/2 \simeq 53$ MeV. The presence of χ -neutrino interaction will modify the COHERENT spectrum, which can be seen in Fig. 3. We select two benchmark points to illustrate the effects of modified spectra:

- Case A: $m_\chi = 10$ MeV, $m_{Z'} = 100$ MeV, and $g_\chi g_q = 5.0 \times 10^{-8}$,
- Case B: $m_\chi = 100$ MeV, $m_{Z'} = 1000$ MeV, and $g_\chi g_q = 5.0 \times 10^{-4}$.

Here we assume $g_{\chi L} = g_{\chi R} = g_\chi$. In case A, the modification to the SM spectrum is dominated by the tree-level scattering process, $\nu N \rightarrow \chi N$, and the loop-level contribution can be neglected due to the small coupling constants. In case B, the tree-level process is kinematically forbidden for $m_\chi \gtrsim 53$ MeV, and the modification to the SM spectrum is only contributed by the loop-level diagrams.

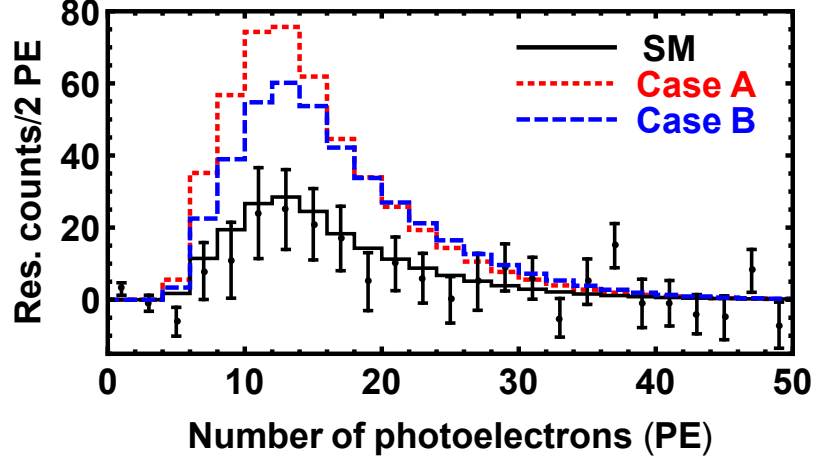


FIG. 3. The expected CE ν NS residual event as a function of the number of photoelectrons at COHERENT. The black solid lines correspond to the SM case, and the red dotted (blue dashed) lines correspond to Case A (B) with $m_\chi = 10$ MeV, $m_{Z'} = 100$ MeV, and $g_\chi g_q = 5.0 \times 10^{-8}$ ($m_\chi = 100$ MeV, $m_{Z'} = 1000$ MeV, and $g_\chi g_q = 5.0 \times 10^{-4}$). Here we assume $g_{\chi L} = g_{\chi R} = g_\chi$.

IV. NUMERICAL RESULTS

We evaluate the statistical significance of new physics beyond the SM by defining

$$\chi^2 = \sum_{i=4}^{15} \left[\frac{N_{\text{meas}}^i - N_{\text{th}}^i(1 + \alpha) - B_{\text{on}}(1 + \beta)}{\sigma_{\text{stat}}^i} \right]^2 + \left(\frac{\alpha}{\sigma_\alpha} \right)^2 + \left(\frac{\beta}{\sigma_\beta} \right)^2, \quad (34)$$

where N_{meas}^i and N_{th}^i are the number of measured and predicted events per energy bin, respectively. Here α (β) is the nuisance parameters for the signal rate (the beam-on background) with an uncertainty of $\sigma_\alpha = 0.28$ ($\sigma_\beta = 0.25$) [1]. The statistical uncertainty per energy bin is given by $\sigma_{\text{stat}}^i = \sqrt{N_{\text{meas}}^i + 2B_{\text{SS}}^i + B_{\text{on}}^i}$ with B_{SS}^i being the steady-state background from the anti-coincident data, and B_{on}^i the beam-on background mainly from prompt neutrons [48].

To obtain the bounds on the simplified neutrino model, we first set $g_{\chi L} = g_{\chi R} = g_\chi$ and $m_{Z'} = 10m_\chi$ or $2m_\chi$ for both case A and B, and scan over possible values of the product of the coefficients $g_\chi g_q$ for a given m_χ . The 90% CL upper bounds on $g_\chi g_q$ as a function of m_χ are shown in Fig. 4. As we see from the top left panel in Fig. 4, for $m_\chi \lesssim 53$ MeV in case A, the scattering is dominated by the tree-level process $\nu N \rightarrow \chi N$ and the upper bounds on $g_\chi g_q$ can reach as small as 6.7×10^{-9} at $m_\chi = 1$ MeV for $m_{Z'} = 10m_\chi$. The bounds become flat at small m_χ region, which can be understood from Eq. (24) since for small m_χ and $m_{Z'}$ the tree-level process will be only sensitive to the coupling constants. For $m_\chi \gtrsim 53$ MeV, however, the tree-level process $\nu N \rightarrow \chi N$ is kinematically forbidden and the relatively weaker bounds are entirely from the loop contributions. Thus, one can see a kink around $m_\chi \simeq 53$ MeV. From the left panels of Fig. 4 to the right panels, in general the bounds become stronger as the mediator mass $m_{Z'}$ decreases. Also,

from the top right panel in Fig. 4, we see that for $m_{Z'} = 2m_\chi$, the loop-level process becomes comparable to the tree-level process for small m_χ , which gives a kink around $m_\chi \simeq 2$ MeV. The upper bounds on $g_\chi g_q$ can reach as small as 1.5×10^{-9} at $m_\chi = 1$ MeV for $m_{Z'} = 2m_\chi$.

We also show the 90% CL upper bounds on $g_\chi g_q$ as a function of m_χ for case B in the bottom panels of Fig. 4. The results are shown in the bottom left and right panel of Fig. 4 for $m_{Z'} = 10m_\chi$ and $m_{Z'} = 2m_\chi$, respectively. From Eq. (16), one can see that the tree-level process in case B has no SI terms and the bounds for CE ν NS are only determined by the loop-level contributions. Unlike case A with pure vector mediator Z' , the case B is induced by axial-vector current between Z' and the SM quarks and has additional contributions from pNGB φ in loop diagrams. The loop-level constraints on the couplings are thus stronger than those in case A. For $m_\chi \simeq 53$ MeV in case B, the pure loop-level contribution constrains $g_\chi g_q$ at the level of 10^{-5} (10^{-6}) for $m_{Z'} = 10m_\chi$ ($2m_\chi$). For small m_χ region, compared with the tree-level process in case A, the loop diagrams have stronger dependence on m_χ as expected.

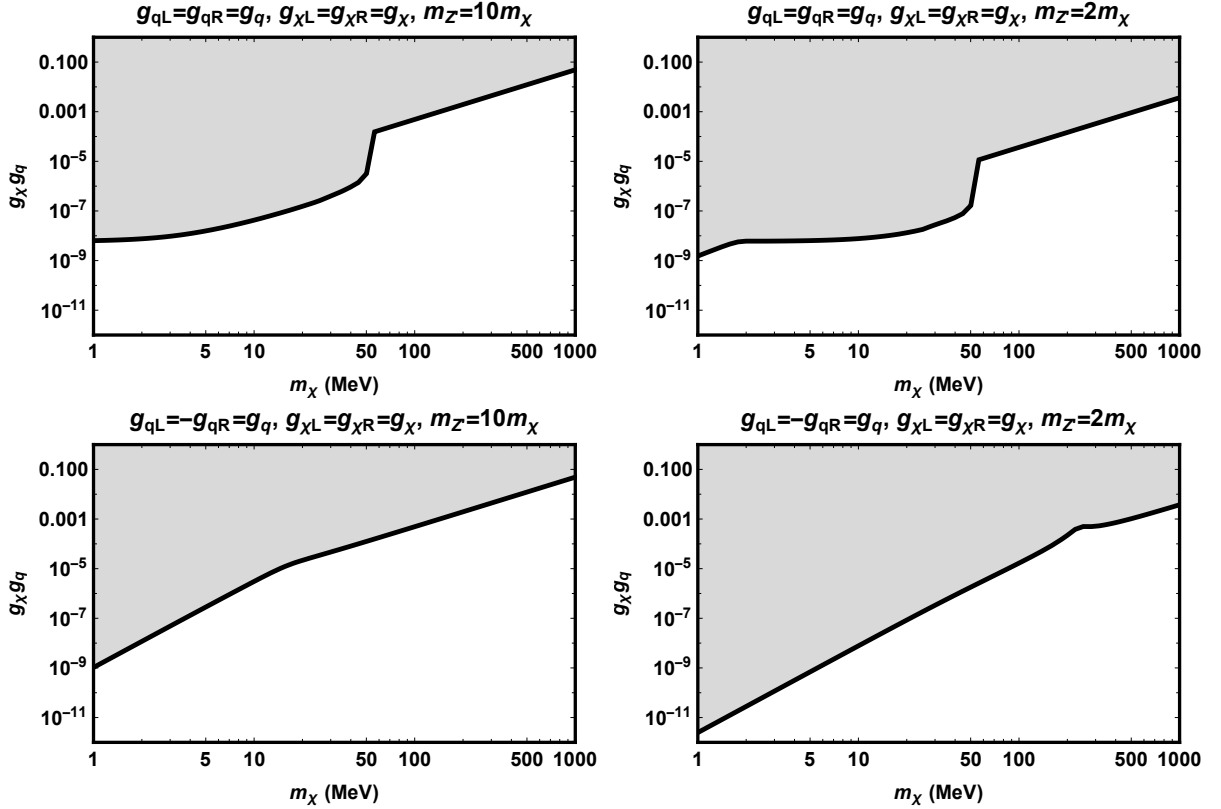


FIG. 4. The 90% CL upper bounds on $g_\chi g_q$ as a function of the mass m_χ from COHERENT. We assume $g_{\chi L} = g_{\chi R} = g_\chi$, $g_{qL} = g_{qR} = g_q$ (top panels: case A) or $g_{qL} = -g_{qR} = g_q$ (bottom panels: case B) and $m_{Z'} = 10m_\chi$ (left), or $m_{Z'} = 2m_\chi$ (right).

V. CONCLUSIONS

We investigate the general neutrino interactions with an exotic fermion χ and a vector mediator in light of the coherent neutrino-nucleus scattering. We consider the framework of a simplified neutrino model in which a new Dirac fermion χ interacts with active neutrinos and a leptophobic vector mediator Z' . The chiral couplings between the mediator and the new fermion χ (the SM quarks) are parameterized by $g_{\chi L}$ and $g_{\chi R}$ (g_{qL} and g_{qR}). At tree-level, the new fermion χ can be produced through the inelastic scattering process $\nu N \rightarrow \chi N$. We also include the loop-level contributions to the CE ν NS process $\nu N \rightarrow \nu N$ with the new fermion χ running in the loop diagrams. For the choice of chiral couplings in the quark sector $g_{qL} = g_{qR}$ ($g_{qL} = -g_{qR}$), the CE ν NS processes are dominated by the tree-level (loop-level) contribution. The COHERENT data are applied to place constraints on the couplings and the mass of fermion χ . We summarize our main conclusions in the following

- For the case of $g_{qL} = g_{qR} = g_q$ with vector current in quark sector, the scattering is mostly dominated by the tree-level process $\nu N \rightarrow \chi N$ for $m_\chi \lesssim 53$ MeV and the upper bounds on $g_\chi g_q$ can reach as small as 6.7×10^{-9} (1.5×10^{-9}) at $m_\chi = 1$ MeV for $m_{Z'} = 10m_\chi$ ($2m_\chi$). For $m_\chi \gtrsim 53$ MeV, the bounds entirely come from the loop process $\nu N \rightarrow \nu N$ and are relatively weaker.
- For the case of $g_{qL} = -g_{qR}$ with axial-vector current, the bounds for CE ν NS are only induced by the loop-level contributions. For $m_\chi \simeq 53$ MeV in this case, the pure loop-level contribution constrains $g_\chi g_q$ at the level of 10^{-5} (10^{-6}) for $m_{Z'} = 10m_\chi$ ($2m_\chi$).

ACKNOWLEDGMENTS

TL is supported by the National Natural Science Foundation of China (Grant No. 11975129, 12035008) and “the Fundamental Research Funds for the Central Universities”, Nankai University (Grant No. 63196013). JL is supported by the National Natural Science Foundation of China (Grant No. 11905299), Guangdong Basic and Applied Basic Research Foundation (Grant No. 2020A1515011479), the Fundamental Research Funds for the Central Universities, and the Sun Yat-Sen University Science Foundation. WC is supported by the National Natural Science Foundation of China under grant No. 11775025 and the Fundamental Research Funds for the Central Universities under grant No. 2017NT17.

Appendix A: Loop diagram calculation

The Passarino-Veltman functions for the one-loop box diagrams are defined as

$$D_0^b \equiv D_0[p_1^2, p_1^2, 0, 0, 0, p_1^2; 0, m_\chi^2, m_{Z'}^2, m_{Z'}^2] = \frac{-m_{Z'}^2 + m_\chi^2 + m_{Z'}^2 \ln\left(\frac{m_{Z'}^2}{m_\chi^2}\right)}{m_{Z'}^2(m_{Z'}^2 - m_\chi^2)^2}, \quad (\text{A1})$$

$$D_{00}^a - D_{00}^b \equiv D_{00}[p_1^2, p_1^2, 0, 0, 0, p_1^2; 0, m_\chi^2, 0, m_{Z'}^2] - D_{00}[p_1^2, p_1^2, 0, 0, 0, p_1^2; 0, m_\chi^2, m_{Z'}^2, m_{Z'}^2] \\ = \frac{m_{Z'}^2 - m_\chi^2 - m_{Z'}^2 \ln\left(\frac{m_{Z'}^2}{m_\chi^2}\right)}{4(m_{Z'}^2 - m_\chi^2)^2}, \quad (\text{A2})$$

$$D_{11}^a - D_{11}^b \equiv D_{11}[p_1^2, p_1^2, 0, 0, 0, p_1^2; 0, m_\chi^2, 0, m_{Z'}^2] - D_{11}[p_1^2, p_1^2, 0, 0, 0, p_1^2; 0, m_\chi^2, m_{Z'}^2, m_{Z'}^2] \\ = m_{Z'}^2 \frac{(m_{Z'}^2 - m_\chi^2)(m_{Z'}^2 + 5m_\chi^2) - 2m_\chi^2(2m_{Z'}^2 + m_\chi^2) \ln\left(\frac{m_{Z'}^2}{m_\chi^2}\right)}{6m_\chi^2(m_{Z'}^2 - m_\chi^2)^4}, \quad (\text{A3})$$

$$D_{001}^a - D_{001}^b \equiv D_{001}[p_1^2, p_1^2, 0, 0, 0, p_1^2; 0, m_\chi^2, 0, m_{Z'}^2] - D_{001}[p_1^2, p_1^2, 0, 0, 0, p_1^2; 0, m_\chi^2, m_{Z'}^2, m_{Z'}^2] \\ = m_{Z'}^2 \frac{-2m_{Z'}^2 + 2m_\chi^2 + (m_{Z'}^2 + m_\chi^2) \ln\left(\frac{m_{Z'}^2}{m_\chi^2}\right)}{12(m_{Z'}^2 - m_\chi^2)^3}, \quad (\text{A4})$$

$$D_1^b \equiv D_1[p_1^2, p_1^2, 0, 0, 0, p_1^2; 0, m_\chi^2, m_{Z'}^2, m_{Z'}^2] = \frac{2(m_{Z'}^2 - m_\chi^2) - (m_{Z'}^2 + m_\chi^2) \ln\left(\frac{m_{Z'}^2}{m_\chi^2}\right)}{2(m_{Z'}^2 - m_\chi^2)^3} \quad (\text{A5})$$

$$D_{00}^b \equiv D_{00}[p_1^2, p_1^2, 0, 0, 0, p_1^2; 0, m_\chi^2, m_{Z'}^2, m_{Z'}^2] = \frac{-m_{Z'}^2 + m_\chi^2 + m_\chi^2 \ln\left(\frac{m_{Z'}^2}{m_\chi^2}\right)}{4(m_{Z'}^2 - m_\chi^2)^2}, \quad (\text{A6})$$

The F_G function for the two-loop diagrams with two pNGB φ mediators in case B is

$$F_G(p_1^2, m_\chi^2, m_{Z'}^2, m_q^2) = \int_0^1 dx \left[-3 \frac{\partial}{\partial m_{Z'}^2} X_1\left(p_1^2, m_\chi^2, m_{Z'}^2, \frac{m_q^2}{x(1-x)}\right) \right. \\ + \frac{3m_q^2(1+x-x^2)}{x^2(1-x)^2} \frac{\partial}{\partial m_{Z'}^2} X_2\left(p_1^2, m_\chi^2, m_{Z'}^2, \frac{m_q^2}{x(1-x)}\right) \\ \left. - \frac{4m_q^4(1-3x+3x^2)}{x^3(1-x)^3} \frac{\partial}{\partial m_{Z'}^2} X_3\left(p_1^2, m_\chi^2, m_{Z'}^2, \frac{m_q^2}{x(1-x)}\right) \right], \quad (\text{A7})$$

where

$$X_1\left(p_1^2, m_\chi^2, m_{Z'}^2, \frac{m_q^2}{x(1-x)}\right) = \frac{1}{m_{Z'}^2 - \frac{m_q^2}{x(1-x)}} \left[B_0(p_1^2, m_{Z'}^2, m_\chi^2) - B_0\left(p_1^2, \frac{m_q^2}{x(1-x)}, m_\chi^2\right) \right], \quad (\text{A8})$$

$$X_2\left(p_1^2, m_\chi^2, m_{Z'}^2, \frac{m_q^2}{x(1-x)}\right) = \frac{1}{m_{Z'}^2 - \frac{m_q^2}{x(1-x)}} \left[X_1\left(p_1^2, m_\chi^2, m_{Z'}^2, \frac{m_q^2}{x(1-x)}\right) - C_0\left(p_1^2, \frac{m_q^2}{x(1-x)}, m_\chi^2\right) \right], \quad (\text{A9})$$

$$X_3\left(p_1^2, m_\chi^2, m_{Z'}^2, \frac{m_q^2}{x(1-x)}\right) = \frac{1}{m_{Z'}^2 - \frac{m_q^2}{x(1-x)}} \left[X_2\left(p_1^2, m_\chi^2, m_{Z'}^2, \frac{m_q^2}{x(1-x)}\right) - D_0\left(p_1^2, \frac{m_q^2}{x(1-x)}, m_\chi^2\right) \right], \quad (\text{A10})$$

and

$$\int \frac{d^4\ell}{(2\pi)^4} \frac{1}{[(\ell+p)^2 - M^2](\ell^2 - m^2)} = \frac{i}{(4\pi)^2} B_0(p^2, m^2, M^2), \quad (\text{A11})$$

$$\int \frac{d^4\ell}{(2\pi)^4} \frac{1}{[(\ell+p)^2 - M^2](\ell^2 - m^2)^2} = \frac{i}{(4\pi)^2} C_0(p^2, m^2, M^2), \quad (\text{A12})$$

$$\int \frac{d^4\ell}{(2\pi)^4} \frac{1}{[(\ell+p)^2 - M^2](\ell^2 - m^2)^3} = \frac{i}{(4\pi)^2} D_0(p^2, m^2, M^2) . \quad (\text{A13})$$

-
- [1] D. Akimov *et al.* (COHERENT), *Science* **357**, 1123 (2017), [arXiv:1708.01294 \[nucl-ex\]](#).
 - [2] D. Z. Freedman, *Phys. Rev. D* **9**, 1389 (1974).
 - [3] V. Brdar, W. Rodejohann, and X.-J. Xu, *JHEP* **12**, 024 (2018), [arXiv:1810.03626 \[hep-ph\]](#).
 - [4] W.-F. Chang and J. Liao, *Phys. Rev. D* **102**, 075004 (2020), [arXiv:2002.10275 \[hep-ph\]](#).
 - [5] N. Hurtado, H. Mir, I. M. Shoemaker, E. Welch, and J. Wyenberg, *Phys. Rev. D* **102**, 015006 (2020), [arXiv:2005.13384 \[hep-ph\]](#).
 - [6] V. Brdar, A. Greljo, J. Kopp, and T. Opferkuch, *JCAP* **01**, 039 (2021), [arXiv:2007.15563 \[hep-ph\]](#).
 - [7] D. Z. Freedman, D. N. Schramm, and D. L. Tubbs, *Ann. Rev. Nucl. Part. Sci.* **27**, 167 (1977).
 - [8] M. Drees and M. Nojiri, *Phys. Rev. D* **48**, 3483 (1993), [arXiv:hep-ph/9307208](#).
 - [9] J. Hisano, K. Ishiwata, and N. Nagata, *Phys. Rev. D* **82**, 115007 (2010), [arXiv:1007.2601 \[hep-ph\]](#).
 - [10] S. Baek, P. Ko, and P. Wu, *JHEP* **10**, 117 (2016), [arXiv:1606.00072 \[hep-ph\]](#).
 - [11] S. Baek, P. Ko, and P. Wu, *JCAP* **07**, 008 (2018), [arXiv:1709.00697 \[hep-ph\]](#).
 - [12] G. Arcadi, M. Lindner, F. S. Queiroz, W. Rodejohann, and S. Vogl, *JCAP* **03**, 042 (2018), [arXiv:1711.02110 \[hep-ph\]](#).
 - [13] T. Li, *Phys. Lett. B* **782**, 497 (2018), [arXiv:1804.02120 \[hep-ph\]](#).
 - [14] T. Abe, M. Fujiwara, and J. Hisano, *JHEP* **02**, 028 (2019), [arXiv:1810.01039 \[hep-ph\]](#).
 - [15] T. Abe *et al.* (LHC Dark Matter Working Group), *Phys. Dark Univ.* **27**, 100351 (2020), [arXiv:1810.09420 \[hep-ex\]](#).
 - [16] T. Li and P. Wu, *Chin. Phys. C* **43**, 113102 (2019), [arXiv:1904.03407 \[hep-ph\]](#).
 - [17] K. A. Mohan, D. Sengupta, T. M. Tait, B. Yan, and C.-P. Yuan, *JHEP* **05**, 115 (2019), [arXiv:1903.05650 \[hep-ph\]](#).
 - [18] F. Ertas and F. Kahlhoefer, *JHEP* **06**, 052 (2019), [arXiv:1902.11070 \[hep-ph\]](#).
 - [19] F. Giacchino, A. Ibarra, L. Lopez Honorez, M. H. G. Tytgat, and S. Wild, *JCAP* **02**, 002 (2016), [arXiv:1511.04452 \[hep-ph\]](#).
 - [20] F. Giacchino, L. Lopez-Honorez, and M. H. Tytgat, *JCAP* **08**, 046 (2014), [arXiv:1405.6921 \[hep-ph\]](#).
 - [21] A. Ibarra, T. Toma, M. Totzauer, and S. Wild, *Phys. Rev. D* **90**, 043526 (2014), [arXiv:1405.6917 \[hep-ph\]](#).
 - [22] S. Colucci, B. Fuks, F. Giacchino, L. Lopez Honorez, M. H. Tytgat, and J. Vandecasteele, *Phys. Rev. D* **98**, 035002 (2018), [arXiv:1804.05068 \[hep-ph\]](#).
 - [23] S. Colucci, F. Giacchino, M. H. Tytgat, and J. Vandecasteele, *Phys. Rev. D* **98**, 115029 (2018), [arXiv:1805.10173 \[hep-ph\]](#).
 - [24] W. Chao, *JHEP* **11**, 013 (2019), [arXiv:1904.09785 \[hep-ph\]](#).
 - [25] T. Li and J. Liao, *JHEP* **02**, 099 (2021), [arXiv:2008.00743 \[hep-ph\]](#).
 - [26] L. Lavoura, *Eur. Phys. J. C* **29**, 191 (2003), [arXiv:hep-ph/0302221](#).

- [27] M. J. Dolan, F. Kahlhoefer, C. McCabe, and K. Schmidt-Hoberg, *JHEP* **03**, 171 (2015), [Erratum: *JHEP* 07, 103 (2015)], [arXiv:1412.5174 \[hep-ph\]](#).
- [28] E. Cortina Gil *et al.* (NA62), (2020), [arXiv:2007.08218 \[hep-ex\]](#).
- [29] J. J. Bennett, G. Buldgen, M. Drewes, and Y. Y. Y. Wong, *JCAP* **03**, 003 (2020), [Addendum: *JCAP* 03, A01 (2021)], [arXiv:1911.04504 \[hep-ph\]](#).
- [30] M. Escudero Abenza, *JCAP* **05**, 048 (2020), [arXiv:2001.04466 \[hep-ph\]](#).
- [31] J. J. Bennett, G. Buldgen, P. F. De Salas, M. Drewes, S. Gariazzo, S. Pastor, and Y. Y. Y. Wong, (2020), [arXiv:2012.02726 \[hep-ph\]](#).
- [32] K. N. Abazajian *et al.* (CMB-S4), (2016), [arXiv:1610.02743 \[astro-ph.CO\]](#).
- [33] K. Abazajian *et al.*, (2019), [arXiv:1907.04473 \[astro-ph.IM\]](#).
- [34] A. Boyarsky, M. Ovchinnikov, N. Sabti, and V. Syvolap, (2021), [arXiv:2103.09831 \[hep-ph\]](#).
- [35] M. A. Shifman, *Nucl. Phys. B* **173**, 13 (1980).
- [36] V. Novikov, M. A. Shifman, A. Vainshtein, and V. I. Zakharov, *Fortsch. Phys.* **32**, 585 (1984).
- [37] W. Kummer and J. Weiser, *Z. Phys. C* **31**, 105 (1986).
- [38] R. Delbourgo and Triyanta, *Int. J. Mod. Phys. A* **7**, 5833 (1992).
- [39] T. Abe and R. Sato, *JHEP* **03**, 109 (2015), [arXiv:1501.04161 \[hep-ph\]](#).
- [40] J. Hisano, (2017), [10.1093/oso/9780198855743.003.0011](#), [arXiv:1712.02947 \[hep-ph\]](#).
- [41] M. Cirelli, E. Del Nobile, and P. Panci, *JCAP* **10**, 019 (2013), [arXiv:1307.5955 \[hep-ph\]](#).
- [42] F. Bishara, J. Brod, B. Grinstein, and J. Zupan, *JHEP* **11**, 059 (2017), [arXiv:1707.06998 \[hep-ph\]](#).
- [43] M. Cadeddu, C. Giunti, Y. Li, and Y. Zhang, *Phys. Rev. Lett.* **120**, 072501 (2018), [arXiv:1710.02730 \[hep-ph\]](#).
- [44] D. Aristizabal Sierra, J. Liao, and D. Marfatia, *JHEP* **06**, 141 (2019), [arXiv:1902.07398 \[hep-ph\]](#).
- [45] R. H. Helm, *Phys. Rev.* **104**, 1466 (1956).
- [46] G. Belanger, F. Boudjema, A. Pukhov, and A. Semenov, *Comput. Phys. Commun.* **180**, 747 (2009), [arXiv:0803.2360 \[hep-ph\]](#).
- [47] G. Belanger, F. Boudjema, A. Goudelis, A. Pukhov, and B. Zaldivar, *Comput. Phys. Commun.* **231**, 173 (2018), [arXiv:1801.03509 \[hep-ph\]](#).
- [48] D. Akimov *et al.* (COHERENT), (2018), [10.5281/zenodo.1228631](#), [arXiv:1804.09459 \[nucl-ex\]](#).